Published as:
Beggan, J. P.; Krasnikov, S. A.; Sergeeva, N. N.; Senge, M. O.; Cafolla, A. A. (2012):
Control of the axial coordination of a surface-confined manganese(III) porphyrin complex.
Nanotechnology **23**, 235606 (10pp).

John P. Beggan [†,] *, Sergey A. Krasnikov [†], Natalia N. Sergeeva [‡], Mathias O. Senge [‡] and Attilio A. Cafolla [†].

[†] School of Physical Sciences, Dublin City University, Glasnevin, Dublin 9, Ireland;
[‡] School of Chemistry, SFI Tetrapyrrole Laboratory, Trinity College Dublin, Dublin 2, Ireland.

* Address correspondence to johnpatrick.beggan2@mail.dcu.ie

Abstract

The organisation and thermal lability of chloro(5,10,15,20-tetraphenylporphyrinato)manganese(III) (Cl-MnTPP) molecules on the Ag(111) surface have been investigated under ultra-high-vaccum conditions, using scanning tunnelling microscopy, low energy electron diffraction and x-ray photoelectron spectroscopy. The Cl-MnTPP molecules are found to self-assemble on Ag(111) surface at room-temperature, forming an ordered molecular overlayer described by a square unit cell. In accordance with the three-fold symmetry of the Ag(111) surface, three rotationally equivalent domains of the molecular overlayer are observed. The primitive lattice vectors of the Cl-MnTPP overlayer show an azimuthal rotation of ± 15° [esd's???] relative to that of the Ag(111) surface, while the principle molecular axes of the individual molecules are found to be aligned with the substrate $\langle 10\bar{1} \rangle$ and $\langle \bar{1}2\bar{1} \rangle$ crystallographic directions. The axial chloride (Cl) ligand is found to be orientated away from the Ag(111) surface, whereby the average plane of the porphyrin macrocycle lies parallel to that of the substrate. When adsorbed on the Ag(111) surface, the Cl-MnTTP molecules display a latent thermal lability resulting in the dissociation of the axial Cl ligand at ~ 423 K. The thermally induced dissociation of the Cl ligand leaves the porphyrin complex otherwise intact, giving rise to the coordinatively unsaturated Mn(III) derivative. Consistent with the surface conformation of the Cl-MnTPP precursor, the resulting (5,10,15,20-tetraphenylporphyrinato)manganese(III) (MnTPP) molecules [if the Cl is now gone it cannot be a molecule but be a cation, or does the surface now function as the negative counter ion?] display the same lattice structure and registry with Ag(111) surface.

Introduction

The functional versatility of porphyrins and metalloporphyrins is uniquely related to their conformational flexibility.[1] Though this flexibility allows for nonplanar deformations, the parent functional group, porphine, is essentially flat, due to the extended π conjugation of the macrocycle.[2] Taken together, these properties make porphyrins and their metalated derivatives particularly well suited to surface functionalisation. The extended π system of the porphyrin macrocycle tends to lead to flat surface geometries,[3,4] and in so doing permits lateral interaction, through which self-organisation can occur. Peripheral substitution of the macrocycle allows for the fine tuning of the molecular conformation and, hence, the physicochemical properties of the porphyrin.[5] In this respect, the archetypal substituted porphyrin, 5,10,15,20-tetraphenylporphyrin, and its related homologues, have received much attention.[6–12]

The rich coordination chemistry of manganese porphyrins makes them ideal candidates for a wide range of chemically responsive applications.[13] Complexes of manganese porphyrins are known to catalyse the halogenation of aliphatic substrates,[14] and have shown high reactivity toward alkene epoxidation.[15] Recently, STM imaging of individual manganese porphyrin catalysts at a liquid-solid interface was reported, wherein, the formation of an oxomanganese porphyrin intermediate was visualized prior to the chemical transformation of alkenes into epoxides.[16]

Concerning the Cl-MnTPP molecule, the metal-bound Cl ligand maintains the central manganese ion in the stable +3 oxidation state.[17] The manganese(II) porphyrin would otherwise rapidly and irreversibly oxidise under ambient conditions. The resulting axial asymmetry, allows for two distinct surface conformations of the Cl-MnTPP molecule; namely, an upward or downward orientation of the Cl ligand with respect to the substrate. Hence, an understanding of the axial interactions of the Cl-MnTPP molecule at the vacuum interface necessitates a fundamental knowledge of the corresponding substrate interface. In this manner, the decisive factor governing coordination properties of the central manganese ion is the ability to selectively dissociate the axial Cl ligand.

In the present work, vapour deposited Cl-MnTPP molecules (Figure 1) on the Ag(111) surface, are examined by using scanning tunnelling microscopy (STM), low energy electron diffraction (LEED) and X-ray photoelectron spectroscopy (XPS). STM and LEED are used in order to determine the structure of the molecular overlayer and its registry with the substrate. Combining these techniques with XPS, the surface conformation of the individual molecules is revealed. Element specific and chemical state information obtained by means of XPS, are used to confirm the thermally induced cleavage of the metal-ligand bond, and the integrity of the resulting manganese complex.

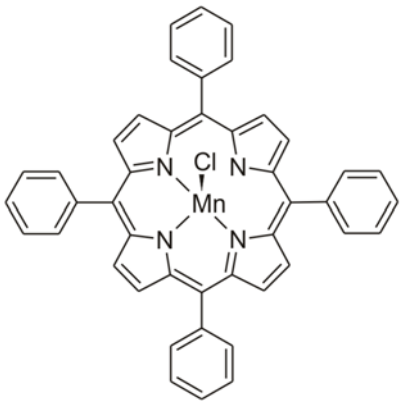

Figure 1. Structural formula of the Cl-MnTPP molecule.

Results and Discussion

Molecular organisation: self-assembly and registry with the Ag(111) surface

Upon deposition, the Cl-MnTPP molecules undergo two-dimensional self-assembly on the Ag(111) surface. Figure 2(a) shows a typical occupied state STM image of the highly ordered lattice structure formed at monolayer coverage. The inset shows an enlarged view, in which an individual molecule is highlighted. The Cl-MnTPP lattice is described by a square unit cell (Fig. 2(a) inset); the lengths of the primitive lattice vectors (b1 and b2) are equal to 1.41 ± 0.05 nm, while the subtended angle is 90 ± 2°. This lattice structure has also been reported for the first layer of CoTPP on both the Ag(111)[18,19] and Au(111)[20] surfaces, while on the latter, it is found to be adopted by Ni- and Cu-TPP.[20] Hence, the ordering of the Cl-MnTTP molecules reflects that typically observed for metallo-TPPs on low reactivity surfaces, with corresponding high mobility and strong lateral intermolecular interaction. Within a single domain, the principle molecular axes of the individual Cl-MnTTP molecules (here defined along the lines of apposing pyrrole groups – see below), are found to be in parallel alignment, and together show an azimuthal rotation of ± 15 ± 2° relative to the primitive lattice vectors of the overlayer unit cell.

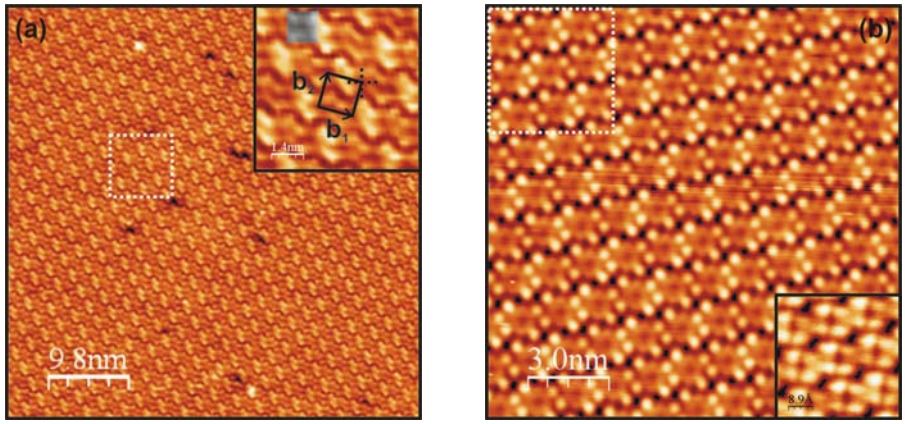

Figure 2. STM images obtained from the Cl-MnTPP monolayer on the Ag(111) surface. (a) Large-scale occupied state STM image; $V_{sample} = -1.20$ V, $I_t = 0.25$ nA, size 50 nm × 50 nm. The inset shows an enlarged view of the region highlighted by the white dotted box; an individual Cl-MnTPP molecule is indicated in grayscale. The unit cell and primitive lattice vectors (b_1, b_2) are shown in black; the principle molecular axes are indicated by the dotted lines. (b) High resolution occupied state STM image; $V_{sample} = -1.20$ V, $I_t = 0.25$ nA, size 15 nm × 15 nm. The inset shows the corresponding unoccupied state STM image of the region highlighted by the white dotted box; $V_{sample} = 1.20$ V, $I_t = 0.25$ nA, size 4.5 nm × 4.5 nm.

In the occupied state STM image of Figure 2(b), the individual molecules show four bright terminal protrusions, between which are found a further set of lesser intensity. Based on the molecular dimensions, the terminal protrusions are attributed to the phenyl groups. In turn, the pyrrole groups of the porphyrin macrocycle, which are located between adjacent phenyl groups, are tentatively assigned to the four core protrusions. Thus, the Cl-MnTTP molecules are seen to adopt an orientation where the average plane of the porphyrin macrocycle lies parallel to that of the Ag(111) surface. In contrast, the unoccupied state STM image shown in the inset reveals a striking difference in the observed intermolecular features. Here the molecular profile is found to be dominated by four lobes localized over the meso-bridge carbons and phenyl groups. This assignment is based on the profile observed in the occupied state image. The observed contrast may be attributed to a difference in the local density of states associated with the occupied and unoccupied molecular orbitals, probed by the applied bias-voltage. A feature common to both molecular profiles, however, is that of a central depression at the porphyrin core. This is especially noteworthy, given the axial asymmetry of the Cl-MnTTP molecule which arises due to Cl ligand, and is discussed below.

Consistent with a planar conformation of the porphyrin macrocycle, the pyrrole groups are found to express approximately the same apparent height. This finding is seemly at odds with the crystallographic structure of the Cl-MnTPP molecule, in which the conformational geometry of the porphyrin macrocycle shows quasi four-fold improper-rotation symmetry.[21] Although such a slight non-planar configuration cannot be ruled out, the apparent planarity of the porphyrin macrocycle may point to a surface induced conformation. In a recent study of (tetraphenylporphyrinato)cobalt(II) on the Cu(111) surface,[22] it was found that the molecular conformation played a decisive role in the observed highest occupied molecular orbital (HOMO). When the molecule presented a planar conformation a HOMO related to the d_z^2 orbital of the central Co atom was found. However, in a saddle conformation, with a larger Co-surface distance, no such relation was observed. Although in the present case, the porphyrin macrocycle exhibits an ostensibly planar conformation, the axial asymmetry of the Mn atom can be expected to strongly influence the tunnelling states localized at the centre of Cl-MnTPP molecule. Here it is noted that XPS spectra obtained from the Cl-MnTPP molecules at monolayer coverage (see below), reveal a chemical environment of the Cl ligand consistent with an upward orientation relative to the Ag(111) surface. In both the crystallographic[21] and calculated[23] structures of the Cl-MnTPP molecule, the Mn atom is found to be displaced from the average plane of the pyrrole

nitrogens, towards the Cl ligand. As the Cl ligand of the adsorbed Cl-MnTPP molecule is found to be orientated away from the Ag(111) surface, the Mn ion can therefore be expected to follow an upward projection. In this context, the depression displayed at the centre of the Cl-MnTPP profile (Fig. 2(b)), is not representative of the actual topographic height. It is therefore tentatively proposed that the displacement of the Mn atom from the Ag(111) surface, brought about by the distorted coordination environment, limits the contribution of molecular orbitals located at the porphyrin core to the tunnelling current; thus, to some degree reflected in the central depression.

Figure 3(a) shows the LEED pattern obtained from approximately 1ML of the Cl-MnTPP molecules on the Ag(111) surface. Twelve first order diffraction spots are observed, equally spaced and equidistant from the central zero order spot. Furthermore, the pattern is found to be invariant with respect 120° rotations, in accordance with the three-fold symmetry of the Ag(111) surface. As such, the pattern is interpreted as being that of a superposition of three rotationally equivalent domains of a square lattice. The individual domains are highlighted (Fig. 3(a)), with the reciprocal lattice vectors of one, given as b^*_1 and b^*_2, with the subtended angle β* equal to 90 ± 2°. The structure of the molecular overlayer displayed by LEED is therefore in good agreement with that observed in STM images.

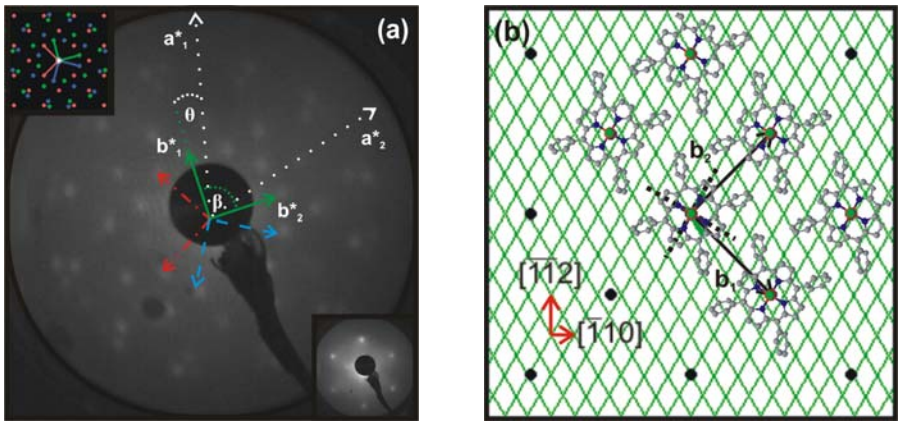

Figure 3. (a) LEED pattern from 1ML of the Cl-MnTPP molecules on the Ag(111) surface acquired at a primary beam energy of 13.(0) eV. The insets shows the LEED pattern of the Ag(111) surface acquired at the higher beam energy of 112.(0) eV (lower) and a simulated LEED pattern of the Cl-MnTPP overlayer created using the observed lattice parameters (upper) (see text). The individual rotational domains of the Cl-MnTPP overlayer are indicated by the green (solid), blue (dashed) and red (dotted/dashed) lines. b^*_1 and b^*_2 are the reciprocal lattice vectors of the rotational domain indicated in green, with the subtended angle given by β*. The dotted white lines labelled a^*_1 and a^*_2 show close packed directions of the Ag(111) reciprocal lattice, whereby the angle θ* indicates the azimuthal rotation of the molecular overlayer. (b) Schematic representation of the azimuthal orientation of the Cl-MnTPP overlayer on the Ag(111) surface. The black dots represent the Cl-MnTPP molecules with the points of intersection of the green mesh that of the Ag atoms. The lattice vectors, labelled b_1 and b_2, of the Cl-MnTPP overlayer are shown in black; the principle molecular axes are indicated by the dotted lines.

The molecular overlayer lattice as revealed in the LEED data, exhibits a preferred orientation to that of the substrate, thus implying an epitaxial relationship. The LEED pattern of the underlying Ag(111) surface is shown in the inset of Figure 3(a).A comparison of the molecular overlayer and substrate LEED patterns reveals their relative orientation. This is visualised in Figure 3(a), where the close-packed directions of the substrate reciprocal lattice are shown superimposed on that of the molecular overlayer pattern. Within this framework, the principal lattice vector (b^*_1) of the overlayer shows an azimuthal rotation θ* of 15° ± 2° relative to that of the substrate (a^*_1). In turn, one diagonal of the molecular overlayer unit cell is found to be aligned with the $\langle \bar{1}10 \rangle$ close-packed directions, while

the other follows the $\langle 11\bar{2} \rangle$ crystallographic directions. Accordingly, the lattice vectors of the molecular overlayer may be expressed in terms of those of the substrate through the following transformation:

$$\begin{pmatrix} b_1 \\ b_2 \end{pmatrix} = \begin{pmatrix} 5.44 & 1.46 \\ 1.46 & 5.44 \end{pmatrix} \begin{pmatrix} a_1 \\ a_2 \end{pmatrix}$$

where the Ag(111) nearest-neighbour distance is 0.289nm. A schematic representation of the corresponding Cl-MnTPP overlayer lattice (for a single rotational domain) superimposed on that of the Ag(111) surface, is shown in Figure 3(b). The graphic clearly illustrates that, the lattice constants (b_1, b_2) of the molecular overlayer preclude commensurism. However, it can be seen that the corresponding 2x2 super-cell, approaches a coincident registry with the substrate lattice points. In addition, every overlayer lattice point coincides with one of the primitive substrate lattice lines. Therefore, within the uncertainty of the measurement, the nature of the molecule-substrate interface is consistent with that previously described as point on line (POL) coincidence (Ref. 24 and references therein).

Through a comparison with the molecular motif observed in STM images (Fig. 2), the azimuthal orientation of the individual Cl-MnTPP molecules may be directly related to corresponding directions on the Ag(111) surface. This is illustrated in Figure 3(b), whereby the principle molecular axes of individual Cl-MnTTP molecules (depicted by structural models) show the observed 15 ± 2° azimuthal rotation relative to the primitive lattice vectors of the overlayer. In this configuration, while one of the molecular axes is aligned with the $\langle 10\bar{1} \rangle$ close-packed directions of the Ag(111) surface, the other follows the $\langle \bar{1}2\bar{1} \rangle$ crystallographic directions. In turn, a symmetry equivalent configuration is obtained for the mirror azimuthal orientation. Thus, while the primitive lattice vectors of the Cl-MnTPP overlayer show an azimuthal rotation relative to that of the Ag(111) surface, the principle axes of individual molecules are found to be aligned with the substrate high symmetry directions.

The axial asymmetry arising from the Cl ligand allows for two distinct surface conformations of the Cl-MnTPP molecule. Depending on the conformation, the axial Cl ligand may point upwards or downwards with respect to the Ag(111) surface. Since chlorine is known to undergo chemical reaction with the Ag(111) surface,[25] it can be expected that for molecules of the first layer, the chemical environment of the Cl ligand will depend on the substrate conformation. In turn, for molecules of the second layer, the Cl ligand is effectively decoupled from the Ag(111) surface. It follows that the Cl ligand of an upward pointing conformation will have a chemical environment similar to that of a second layer molecule. In this way the molecular conformation on the substrate may be inferred from chemical state of the Cl ligand. The Cl 2p XPS spectrum obtained from a surface coverage of ~ 1ML is shown in Figure 4 (lower). Two photoelectron lines are observed which are assigned to a single Cl 2p spin-orbit doublet, the fit of which yields a binding energy (BE) of 197.3 eV for the $2p_{3/2}$ line, with a spin-orbit splitting of 1.6 eV. The corresponding spectrum acquired at a surface coverage of 2-3 ML is shown in Figure 4 (upper). The initial Cl 2p doublet shows an increase commensurate with that of the increased coverage, however, no additional spectral components are observed. This suggests a single chemical state of the Cl ligand for molecules of the first and second molecular layers. The inference therefore, is that the Cl-MnTPP molecules adsorb on the Ag(111) surface with the Cl ligand pointing upwards. The steric hindrance of the large axial Cl ligand would thus be alleviated, allowing for an increased coupling of the extended molecular π system to the substrate.

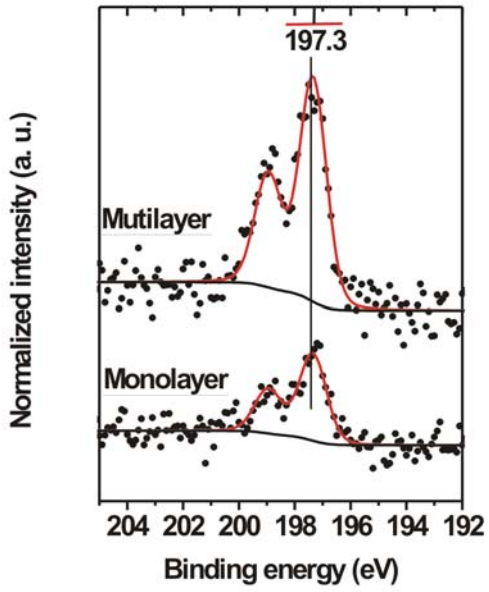

Figure 4. Cl 2p XPS spectra obtained from the Cl-MnTPP overlayer on the Ag(111) surface at a coverage of ~1ML (lower) and ~ 2.5 ML (upper). The dots represent the spectral data. The red and black lines correspond to the best fit to the spectral data and Shirley backgrounds respectively.

Thermal lability: dissociation of the axial Cl ligand

The thermally evaporated Cl-MnTPP molecules adsorb on the Ag(111) surface predominantly intact. The adsorbed Cl-MnTPP molecules are found, however, to display a latent thermal lability which results in the dissociation of the Cl ligand. The onset of Cl dissociation, as reflected in the Cl 2p photoemission intensity, is observed to occur at 423 K. At this temperature, the rate of dissociation is slow, with Cl loss complete only after several hours. Figure 5 shows the C 1s and Cl 2p XPS spectra acquired from ~ 1 ML of the Cl-MnTTP molecules as deposited and, after annealing at 423 K for ~ 15hrs. The initial Cl 2p doublet of the deposited layer is reduced to within the noise level after annealing. However, in the corresponding C1s line a reduction of scarcely 10% is observed. Therefore, the combination of lateral intermolecular and molecule-substrate interactions is strong enough to keep the porphyrin complex adsorbed on the substrate, while the Cl ligand is lost. Recent studies of chloro-manganese porphyrins[26,27] have reported a similar thermal lability of the axial Cl ligand, although occurring at slightly higher temperature (473 K), and achieved by surface tethering via thiol groups.

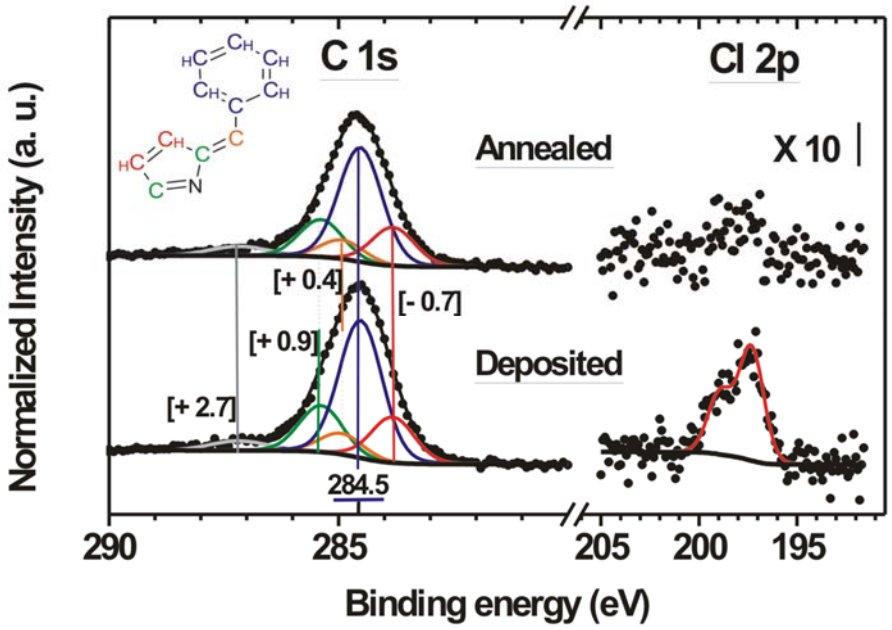

Figure 5. C 1s (left) and Cl 2p (right) XPS spectra obtained from the Cl-MnTPP monolayer on the Ag(111) surface as deposited (lower), and after annealing at 423 K (upper). The dots represent the spectral data. **Left**: The best fit to the spectral data and Shirley background lines are shown in black; the component peaks are colour coded to the non-equivalent carbons shown inset. The bracketed values correspond to shifts in BE of component peaks relative to the peak of largest intensity. **Right** (lower): The red and black lines correspond to the best fit and Shirley background, respectively.

The C1s lineshape, which is observably the same in the XPS spectra of the deposited and annealed layers, is noticeably broadened at the peak base. This finding can be interpreted as being the result of photoemission from chemically distinct carbon species within the porphyrin complex. Guided by the Cl-MnTPP molecular formula, four plausibly different chemical species of carbon atoms can be identified: the meso-bridge carbons (C_m); those of the phenyl groups (C_{ph}); and those at the α and β positions of the pyrrole groups ($C_{N\alpha}$ and $C_{N\beta}$ respectively). Estimation of the relative energy positions of the different spectral contributions, follows a recent report by Nardi et al.[28] on the C1s core level spectrum of TPP; noting however, that the chemical state of the pyrrole nitrogens in metalloporphyrins (Fe, Co, Zn) tends towards that of the azanitrogens in the free-base TPP analogue.[29–31] The resulting fit of the C1s spectra (Fig. 5 lower/upper), yields four principal components. The largest (blue) corresponds to ~ 52% of the total envelope area, and hence is assigned primarily to C_{ph} emission. Two components of equal area (~ 17%), but shifted to higher (green) and lower (red) binding energy, are attributed to $C_{N\alpha}$ and $C_{N\beta}$ emission, respectively. The smallest component (orange) with an area of ~ 8% is thus assigned to C_m emission. A fifth broader component (grey) is included in the fit to accommodate the energy loss structure at higher binding energy,[28] accounting for the somewhat smaller than expected intensity of the principle components. The apparent C1s lineshape, therefore, may be considered to reflect a quasi-fingerprint of the porphyrin complex, thus implying the structure remains intact on loss of the Cl ligand.

The dissociation of the Cl ligand occurs without the demetalation of the porphyrin complex, thus giving rise to an Mn centre that is coordinatively unsaturated. Figure 6 shows the Mn $2p_{3/2}$ XPS spectra obtained from the Cl-MnTPP monolayer as deposited, and after annealing to the complete removal of the Cl ligand. Multiplet splitting of the Mn $2p_{3/2}$ photoelectron lines (Fig. 6), gives rise to their noticeable broadness. The splitting arises when, upon photoemission, the unpaired electron of the core

level couples with those of the open valence shell, resulting in multiple final states. Consequently, the multiplet structure of the Mn $2p_{3/2}$ envelope is sensitive to the number of unpaired electrons in the valence shell, which in turn can be related to the Mn oxidation state.

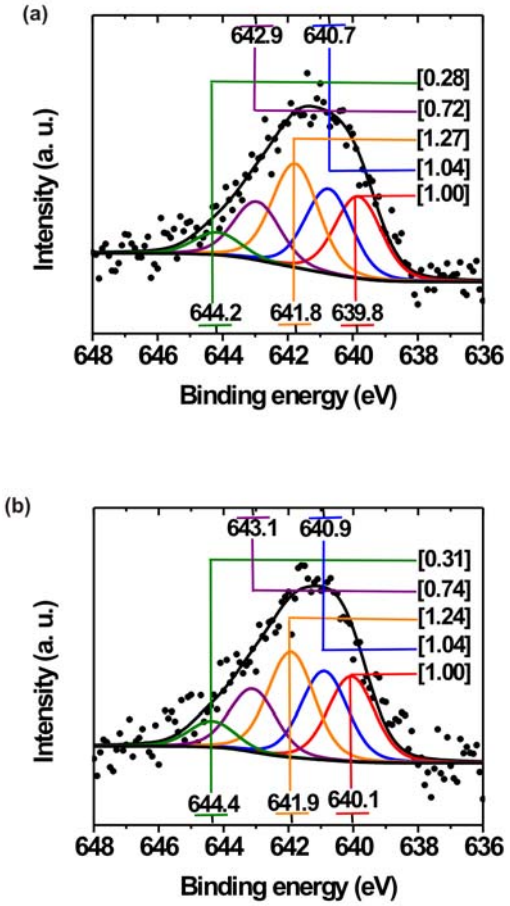

Figure 6. Mn $2p_{3/2}$ XPS spectra obtained from the Cl-MnTPP monolayer on the Ag(111) surface (a) as deposited, and (b) after the complete loss of the Cl ligand. The dots represent the spectral data. The black and grey lines correspond to the best fit to the spectral data and Shirley backgrounds respectively. Peak intensities (bracketed values) are relative to that of lowest binding energy.

Interpretation of the apparent Mn $2p_{3/2}$ lineshape in terms of the underlying multiplet structure follows the calculated multiplet splitting of the Mn 2p vacancy levels, performed by Gupta and Sen.[32] In this respect, the calculated XPS spectra for the Mn +2, +3, and +4 ions have been considered, given that the cleavage of the metal-ligand bond may result in a one electron transfer. This approach has been demonstrated previously;[33] wherein, the essential features of experimentally obtained Mn 2p XPS spectra of Mn +2, +3, and +4 oxides and oxyhydroxides have been reproduced by the calculated multiplet structure. In the present case, however, it should be noted that much of the multiplet structure remains unresolved, due to the weak signal-to-noise ratio of the Mn $2p_{3/2}$ spectra (Fig. 6). This is a consequence of the low number density of the Mn atoms in the molecular monolayer. Even so, the underlying multiplet structure can reasonably be expected to affect the observed Mn $2p_{3/2}$ lineshape and moreover, the binding energy extent of the spectral envelope. Hence, the chemical state of the central Mn atom may be distinguished.

Accordingly, multiplet parameters obtained from the calculated Mn 2p multiplet splitting[32] have been used as initial constraints in the fit of the present Mn $2p_{3/2}$ photoelectron lines. The resulting best-fit of the Mn $2p_{3/2}$ spectrum from the pre-anneal surface (Fig. 4(a)), yields multiplets of relative intensities and energy splittings which are similar to those calculated for the Mn(III) ion.[32] As such, the

spectrum reflects the chemical state of the Mn atom in Cl-MnTPP molecule, which is expected to exist in the +3 oxidation state. In the case of the Mn(III) ion, the calculated multiplet component of lowest binding energy differs from that of the Mn(II) and Mn(IV) ions by +0.7eV and -1.0 eV, respectively.[32] It follows that a change in the oxidation state of the Mn atom, on cleavage of the Cl ligand bond, should result in a clear shift in the binding energy onset Mn $2p_{3/2}$ envelope. However, the onset of the Mn $2p_{3/2}$ envelopes, from the pre- and post-anneal surfaces, occur at approximately the same binding energy. Furthermore, a strikingly similar multiplet structure is obtained in the fit of the Mn $2p_{3/2}$ spectrum from the post-anneal surface (Fig. 6(b)). The implication therefore, is that the thermally induced dissociation of the Cl ligand from the Cl-MnTPP molecules adsorbed on the Ag(111) surface, occurs through a heterolytic cleavage of the metal-ligand bond. As such, the substrate may be expected to compensate for the net charge of the porphyrin complex. The dissociation of the axial ligand in this manner, is in keeping with the relative stabilities of Mn(II) and Mn(III) porphyrins, the latter of which being the most stable.[34]

STM images reveal that the loss of the Mn-bound Cl ligand leaves the porphyrin complex otherwise intact. Accordingly, the indicated Mn(III) complex is confidently assigned to the MnTPP molecule. Figure 7(a) shows typical occupied (main) and unoccupied (inset) state STM images of the MnTPP molecules on the Ag(111) surface at ~ 1ML, following the complete removal of Cl from an equivalent coverage of the deposited Cl-MnTPP. Although without the axial Cl ligand, the MnTPP molecule displays a profile which closely resembles that observed from the Cl-MnTPP precursor (Fig. 2(b)). In the occupied state STM image of Figure 7(a), features associated with the phenyl substituents and porphyrin macrocycle are clearly discernable. In turn, the intramolecular features appear to follow related bias-voltage dependence, as evidenced in the unoccupied state STM image shown inset. Most notably, however, a depression is observed at the porphyrin core, comparable to that displayed by the Cl-MnTPP molecular profile.

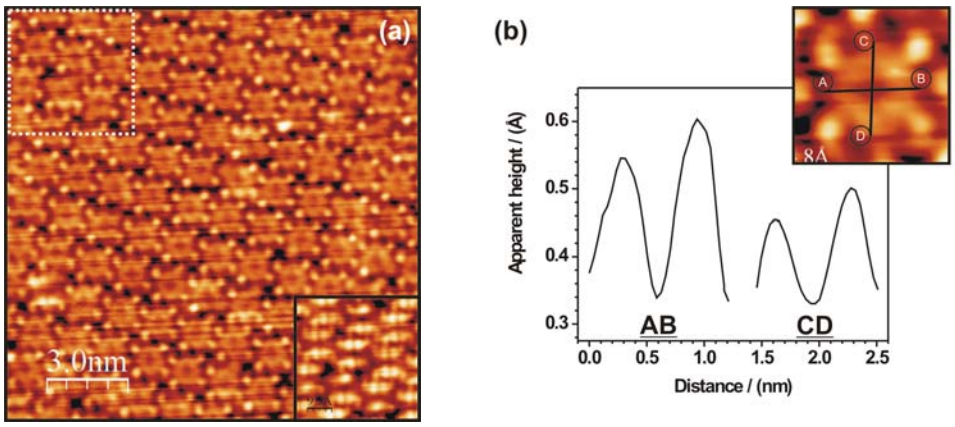

Figure 7. STM images obtained from the MnTPP monolayer on the Ag(111) surface. (a) Occupied state STM image of the MnTPP layer; $V_{sample} = -1.20$ V, $I_t = 0.25$ nA, size 15 nm × 15 nm. The inset shows the corresponding unoccupied state STM image of the region highlighted by the white dotted box; $V_{sample} = 1.20$ V, $I_t = 0.25$ nA, size 4.5 nm × 4.5 nm. (b) Height profiles taken along the lines of opposing pyrrole groups of the MnTPP molecule shown inset.

On close examination of the porphyrin macrocycle (Fig. 7(a)), a slight two-fold rotational symmetry is observed, consistent with a saddle distortion, where two opposite pyrrole groups tilt upwards and two downwards with respect to the surface plane.[35] A corresponding difference in apparent height is shown in figure 7(b), which presents height profiles taken along the lines of opposing pyrrole groups. Although not observed in the case of the Cl-MnTPP precursor, the differences are small enough so as to remain unresolved (Fig. 2(b)). Since the saddle distortion of the Cl-MnTPP porphyrin macrocycle (observed in the crystal structure) is proposed to be brought about by the axial coordination of the Cl ligand,[21] the MnTPP derivative might be expected to adopt a planar configuration. Recent

theoretical predictions[35] show however, that a stabilizing π conjugation exists between the saddled macrocyclic ring and the phenyl groups, as the latter rotate towards the porphyrin plane. Such a conformational distortion of the MnTPP molecule would, presumably, allow for an increased coupling of the molecular π system to the substrate. The observed two-fold symmetry of the porphyrin macrocycle (Fig. 7(b)), therefore, points to a conformational adaptation of the MnTPP molecule, upon adsorption on the Ag(111) surface. Such conformational flexibility of meso-aryl-substituted porphyrins upon adsorption is well established.[36] On the Ag(111) surface, tetrapyridylporphyrin molecules are found to adopt a conformation in which the pyridyl groups are alternately rotated out of the porphyrin plane,[37] whereas in the case of CoTPP, a concerted phenyl rotation and saddling of the macrocycle is observed.[38]

It was proposed that the depression displayed at the centre of the Cl-MnTPP profile (Fig. 2(b)), is not topographic in origin, but rather, arises from intrinsic electronic factors. As mentioned above, the removal of the axial Cl ligand is found to leave the molecular appearance, and thus, conformation, comparatively unchanged - conspicuously so at the porphyrin core (Fig 7). These observations clearly indicate that the MOs localized at the porphyrin macrocycle, remain largely unmixed with the orbitals originating from the Cl ligand. Hence, affecting the molecular profile observed in STM images. This conclusion, is supported by the calculated MO structure of the closely related chloro(tetraphenylporphyrinato)manganese(II) (Cl-Mn(II)TPP) molecule;[39] the results of the which reveal that among the porphyrin π, Mn d, and Cl ligand orbitals little intermixing takes place. It should be noted, however, that a direct comparison between the d^4 Cl-Mn(III)TPP and the d^5 Cl-Mn(II)TPP complexes, may not be fully appropriate. The additional electron of the d^5 Mn complex induces a lengthening of the coordination bonds, further distorting the square pyramidal coordination geometry of the Mn atom.[39] One obvious consequence of this is a reduced overlap of the equatorial (porphyrin) and axial ligand orbitals, which likewise affects their mixing. Consequently, lack of intermixing may be expected to be more pronounced in the case of the d^5 Cl-Mn(II)TPP complex.

Lastly, the ordering of the MnTPP overlayer (Fig. 7) is described by a square unit cell, with dimensions equal to those displayed by the Cl-MnTPP precursor. The LEED pattern obtained (not shown) from the MnTPP molecules on the Ag(111) surface at approximately 1ML, is consistent with that of a square lattice, in good agreement with the structure observed in STM images. Furthermore, the registry of the MnTPP overlayer relative with the Ag(111) substrate, as indicated by LEED, is found to be the same as that observed for the Cl-MnTPP layer. It is evident therefore, that the loss of the Cl ligand has little or no effect on the lateral intermolecular interaction or the specific adsorption site on the Ag(111) surface. Indeed this may be expected given that the Cl ligand is axially bound to the Mn atom, and is found to be orientated away from Ag(111) surface.

Conclusions

The self-assembled Cl-MnTPP layer grows epitaxially on the Ag(111) surface, in a manner consistent with POL coincidence. While the primitive Cl-MnTPP lattice vectors show an azimuthal rotation relative to that of the Ag(111) surface, the principle axes of individual molecules are aligned with the substrate high symmetry directions. The surface conformation of the Cl-MnTPP molecules is such that the axial Cl ligand points upwards relative to the Ag(111) surface. In this conformation the axial binding site at the vacuum interface is occupied by the Cl ligand; thus it can be expected that further axially coordination is inhibited.

When adsorbed on the Ag(111) surface, the MnTPP-Cl molecules display a latent thermal lability which results in the dissociation of the Cl ligand upon annealing. The thermally induced dissociation of the Cl ligand occurs through a heterolytic cleavage of the metal-ligand bond, without the demetalation of the porphyrin complex. Furthermore, the loss of the Cl ligand, has little or no effect, on the resulting overlayer lattice structure or its registry with the Ag(111) surface. In this manner, an ordered array of coordinatively unsaturated MnTPP molecules is created, capable of axial coordination at the vacuum interface.

Methods

The STM, XPS and LEED experiments were conducted in UHV, using a commercial system (Omicron Nanotechnology GmbH) consisting of an analysis chamber (with a base pressure of 9×10^{-11} mbar) and a preparation chamber (1×10^{-10} mbar).

STM imaging was performed at room-temperature, using an Omicron VT STM. Electrochemically etched polycrystalline W tips (Omicron) were used as tunnelling probes. The STM images were recorded in constant-current mode, with the given voltages (V_{sample}) corresponding to the sample-bias with respect to the W tip. The STM data were processed using the WSxM software package.[40]

XPS measurements were carried out using an Omicron ESCA+ spectrometer. The core-level spectra were collected with a hemispherical energy analyzer (EA 125 U5), employing an Al Kα X-ray source (DAR 400). The spectrometer was operated with one of two analyser pass energies, with overall energy resolutions of 1.0 eV and 1.4 eV respectively, the latter in cases where increased sensitivity was required: the Mn 2p core-level spectra; and those of the Cl 2p reported in Figure 5. The core-level binding energies were referenced to the Ag $3d_{5/2}$ line (368.2 eV) of the clean Ag surface. The XPS spectra were analyzed using the FITT 1.2 (GTK) software package (Photoelectron Spectroscopy Lab, Seoul National University).

The LEED diffraction patterns were obtained using an Omicron four grid Spectraleed system, fitted with rear-view optics and LaB_6 filament. Analysis of the diffraction patterns was performed using the LEEDpat 2.1 pattern simulator.[41]

A single-crystal Ag(111) surface (Surface Preparation Laboratory) was used as the substrate. The Ag(111) crystal was cleaned *in situ* by repeated cycles of argon ion sputtering (U = 1 kV) followed by annealing at 850 K, until found to be clean by XPS and STM analysis. The Cl-MnTPP was synthesized according to a published procedure.[42] Prior to deposition, the Cl-MnTPP powder was outgassed below its evaporation temperature. The Cl-MnTTP was subsequently evaporated in a preparation chamber, isolated from the STM chamber, at a rate of about 0.2 ML (monolayer) per minute from a tantalum crucible in a homemade deposition cell operated at a temperature of approximately 600 K. The Ag(111) substrate was maintained at room temperature during the Cl-MnTPP deposition. The Cl-MnTPP surface coverage is defined as number of adsorbed molecules divided by the number in a filled monolayer.

Acknowledgements. This work was supported by grants from Science Foundation Ireland (P.I. 09/IN.1/B2650 and xxxxxTonyxxx)

References

(1) Senge, M. O. Exercises in molecular gymnastics - bending, stretching and twisting porphyrins. *Chem. Commun.* **2006**, 243-256.
(2) Milgrom, L. R. In *The colours of life: an introduction to the chemistry of porphyrins and related compounds;* Oxford University Press: Oxford, 1997.
(3) Beggan, J. P.; Krasnikov, S. A.; Sergeeva, N. N.; Senge, M. O.; Cafolla, A. A. Self-assembly of Ni(II) porphine molecules on the Ag/Si(111)-(root 3 x root 3) R30 degrees surface studied by STM/STS and LEED. *J. Phys.: Condens. Matter* **2008**, *20*, 015003.
(4) Krasnikov, S. A.; Beggan, J. P.; Sergeeva, N. N.; Senge, M. O.; Cafolla, A. A. Ni(II) porphine nanolines grown on a Ag(111) surface at room temperature. *Nanotechnology* **2009**, *20*, 135301.
(5) Barkigia, K. M.; Renner, M. W.; Senge, M. O.; Fajer, J. Interplay of axial ligation, hydrogen bonding, self-assembly, and conformational landscapes in high-spin Ni(II) porphyrins. *J. Phys. Chem. B* **2004**, *108*, 2173-2180.

(5a) Senge, M. O. Prevention of Out-of-Plane Macrocycle Distortion by Thallium in the Sterically Strained 2,3,7,8,12,13,17,18-Octaethyl-5,10,15,20-tetranitroporphyrin. *J. Chem. Soc., Dalton Trans.* **1993**, 3539-3549.
(6) Gottfried, J. M.; Flechtner, K.; Kretschmann, A.; Lukasczyk, T.; Steinruck, H. P. Direct synthesis of a metalloporphyrin complex on a surface. *J. Am. Chem. Soc.* **2006**, *128*, 5644-5645.
(7) Krasnikov, S. A.; Sergeeva, N. N.; Brzhezinskaya, M. M.; Preobrajenski, A. B.; Sergeeva, Y. N.; Vinogradov, N. A.; Cafolla, A. A.; Senge, M. O.; Vinogradov, A. S. An X-ray absorption and photoemission study of the electronic structure of Ni porphyrins and Ni N-confused porphyrin. *J. Phys.: Condens. Matter* **2008**, *20*, 235207.
(8) Buchner, F.; Seufert, K.; Auwaerter, W.; Heim, D.; Barth, J. V.; Flechtner, K.; Gottfried, J. M.; Steinrueck, H.; Marbach, H. NO-Induced Reorganization of Porphyrin Arrays. *ACS Nano* **2009**, *3*, 1789-1794.
(9) Krasnikov, S. A.; Sergeeva, N. N.; Sergeeva, Y. N.; Senge, M. O.; Cafolla, A. A. Self-assembled rows of Ni porphyrin dimers on the Ag(111) surface. *Phys. Chem. Chem. Phys.* **2010**, *12*, 6666–6671.
(10) Écija, D.; Seufert, K.; Heim, D.; Auwärter, W.; Aurisicchio, C.; Fabbro, C.; Bonifazi, D.; Barth, J. V. Hierarchic self-assembly of nanoporous chiral networks with conformationally flexible porphyrins. *ACS Nano* **2010**, *4*, 4936–4942.
(11) Sedona, F.; Di Marino, M.; Sambi, M.; Carofiglio, T.; Lubian, E.; Casarin, M.; Tondello, E. Fullerene/porphyrin multicomponent nanostructures on Ag(110): from supramolecular self-assembly to extended copolymers. *ACS Nano* **2010**, *4*, 5147–5154.
(12) Krasnikov, S. A.; Doyle, C. M.; Sergeeva, N. N.; Preobrajenski, A. B.; Vinogradov, N. A.; Sergeeva, Y. N.; Zakharov, A. A.; Senge, M. O.; Cafolla, A. A. Formation of extended covalently bonded Ni porphyrin networks on the Au(111) surface. *Nano Res.* **2011**, *4*, 376-384.
(13) K. M. Kadish, K. M. Schmith, and R. Guilard, Ed.; *The Porphyrin Handbook, Applications: Past, Present and Future;* Academic Press: San Diego, 2000; Vol. 6.
(14) Liu, W.; Groves, J. T. Manganese Porphyrins Catalyze Selective C-H Bond Halogenations. *J. Am. Chem. Soc.* **2010**, *132*, 12847-12849.
(15) Groves, J. T. Reactivity and mechanisms of metalloporphyrin-catalyzed oxidations. *J. Porph. Phthal.* **2000**, *4*, 350-352.
(16) Hulsken, B.; Van Hameren, R.; Gerritsen, J. W.; Khoury, T.; Thordarson, P.; Crossley, M. J.; Rowan, A. E.; Nolte, R. J. M.; Elemans, J. A. A. W.; Speller, S. Real-time single-molecule imaging of oxidation catalysis at a liquid-solid interface. *Nat. Nanotechnol.* **2007**, *2*, 285-289.
(17) Boucher, L. J. Manganese Porphyrin Complexes .5. Axial Interactions in Manganese(iii) Porphyrins. *Ann. N. Y. Acad. Sci.* **1973**, *206*, 409-419.
(18) Auwaerter, W.; Seufert, K.; Klappenberger, F.; Reichert, J.; Weber-Bargioni, A.; Verdini, A.; Cvetko, D.; Dell'Angela, M.; Floreano, L.; Cossaro, A.; Bavdek, G.; Morgante, A.; Seitsonen, A. P.; Barth, J. V. Site-specific electronic and geometric interface structure of Co-tetraphenyl-porphyrin layers on Ag(111). *Phys. Rev. B* **2010**, *81*, 245403.
(19) Comanici, K.; Buchner, F.; Flechtner, K.; Lukasczyk, T.; Gottfried, J. M.; Steinrueck, H.; Marbach, H. Understanding the contrast mechanism in scanning tunneling microscopy (STM) images of an intermixed tetraphenylporphyrin layer on Ag(111). *Langmuir* **2008**, *24*, 1897-1901.
(20) Scudiero, L.; Barlow, D. E.; Hipps, K. W. Physical properties and metal ion specific scanning tunneling microscopy images of metal(II) tetraphenylporphyrins deposited from vapor onto gold (111). *J. Phys. Chem. B* **2000**, *104*, 11899-11905.
(21) Tulinsky, A.; Chen, B. M. L. Crystal and Molecular-Structure of Chloro-Alpha,beta,gamma,delta - "Tetraphenylporphinatomanganese(iii). *J. Am. Chem. Soc.* **1977**, *99*, 3647-3651.
(22) Iancu, V.; Deshpande, A.; Hla, S. W. Manipulating Kondo temperature via single molecule switching. *Nano Lett.* **2006**, *6*, 820-823.
(23) Curet-Arana, M. C.; Emberger, G. A.; Broadbelt, L. J.; Snurr, R. Q. Quantum chemical determination of stable intermediates for alkene epoxidation with Mn-porphyrin catalysts. *J. Mol. Catal. A-Chem.* **2008**, *285*, 120-127.

(24) Hooks, D. E.; Fritz, T.; Ward, M. D. Epitaxy and molecular organization on solid substrates. *Adv. Mater.* **2001**, *13*, 227-241.
(25) Lambert, R. M.; Cropley, R. L.; Husain, A.; Tikhov, M. S. Halogen-induced selectivity in heterogeneous epoxidation is an electronic effect - fluorine, chlorine, bromine and iodine in the Ag-catalysed selective oxidation of ethene. *Chem. Commun.* **2003**, 1184-1185.
(26) Turner, M.; Vaughan, O. P. H.; Kynakou, G.; Watson, D. J.; Scherer, L. J.; Papageorgiou, A. C.; Sanders, J. K. M.; Lambert, R. M. Deprotection, Tethering, and Activation of a One-Legged Metalloporphyrin on a Chemically Active Metal Surface: NEXAFS, Synchrotron XPS, and STM Study of [SAc]P-Mn(III)Cl on Ag(100). *J. Am. Chem. Soc.* **2009**, *131*, 14913-14919.
(27) Turner, M.; Vaughan, O. P. H.; Kyriakou, G.; Watson, D. J.; Scherer, L. J.; Davidson, G. J. E.; Sanders, J. K. M.; Lambert, R. M. Deprotection, Tethering, and Activation of a Catalytically Active Metalloporphyrin to a Chemically Active Metal Surface: [SAc](4)P-Mn(III)Cl on Ag(100). *J. Am. Chem. Soc.* **2009**, *131*, 1910-1914.
(28) Nardi, M.; Verucchi, R.; Corradi, C.; Pola, M.; Casarin, M.; Vittadini, A.; Iannotta, S. Tetraphenylporphyrin electronic properties: a combined theoretical and experimental study of thin films deposited by SuMBD. *Phys. Chem. Chem. Phys.* **2010**, *12*, 871-880.
(29) Buchner, F.; Flechtner, K.; Bai, Y.; Zillner, E.; Kellner, I.; Steinrueck, H.; Marbach, H.; Gottfried, J. M. Coordination of iron atoms by tetraphenylporphyrin monolayers and multilayers on Ag(111) and formation of iron-tetraphenylporphyrin. *J. Phys. Chem. C* **2008**, *112*, 15458-15465.
(30) Lukasczyk, T.; Flechtner, K.; Merte, L. R.; Jux, N.; Maier, F.; Gottfried, J. M.; Steinrueck, H. Interaction of cobalt(II) tetraarylporphyrins with a Ag(111) surface studied with photoelectron spectroscopy. *J. Phys. Chem. C* **2007**, *111*, 3090-3098.
(31) Kretschmann, A.; Walz, M.; Flechtner, K.; Steinrueck, H.; Gottfried, J. M. Tetraphenylporphyrin picks up zinc atoms from a silver surface. *Chem. Commun.* **2007**, 568-570.
(32) Gupta, R. P.; Sen, S. K. Calculation of Multiplet Structure of Core P-Vacancy Levels. *Phys. Rev. B* **1975**, *12*, 15-19.
(33) Nesbitt, H. W.; Banerjee, D. Interpretation of XPS Mn(2p) spectra of Mn oxyhydroxides and constraints on the mechanism of MnO2 precipitation. *Am. Mineral.* **1998**, *83*, 305-315.
(34) Boucher, L. J. Manganese Porphyrin Complexes. *Coord. Chem. Rev.* **1972**, *7*, 289-329.
(35) Rosa, A.; Ricciardi, G.; Baerends, E. J. Synergism of porphyrin-core saddling and twisting of meso-aryl substituents. *J. Phys. Chem. A* **2006**, *110*, 5180-5190.
[➔this effect has been known for a long time from X-ray structure papers: e.g.:]
(35a) Senge, M. O.; Forsyth, T. P.; Nguyen, L. T.; Smith, K. M. Sterically Strained Porphyrins. Influence of Core Protonation Versus Peripheral Substitution on the Conformation of Tetra-meso-, Octa-β-, and Dodecasubstituted Porphyrin Dications. *Angew. Chem. Int. Ed.* **1994**, *33*, 2485-2487.
(35b) Kalisch, W. W.; Senge, M. O. Synthesis and Structural Characterization of Nonplanar Tetraphenylporphyrins with Graded Degree of β-Ethyl Substitution. *Tetrahedron Lett.* **1996**, *37*, 1183-1186.
(36) Buchner, F.; Comanici, K.; Jux, N.; Steinrueck, H.; Marbach, H. Polymorphism of porphyrin molecules on Ag(111) and how to weave a rigid monolayer. *J. Phys. Chem. C* **2007**, *111*, 13531-13538.
(37) Auwarter, W.; Weber-Bargioni, A.; Riemann, A.; Schiffrin, A.; Groning, O.; Fasel, R.; Barth, J. V. Self-assembly and conformation of tetrapyridyl-porphyrin molecules on Ag(111). *J. Chem. Phys.* **2006**, *124*, 194708.
(38) Buchner, F.; Warnick, K.; Woelfle, T.; Goerling, A.; Steinrueck, H.; Hieringer, W.; Marbach, H. Chemical Fingerprints of Large Organic Molecules in Scanning Tunneling Microscopy: Imaging Adsorbate-Substrate Coupling of Metalloporphyrins. *J. Phys. Chem. C* **2009**, *113*, 16450-16457.
(39) Vanatta, R. B.; Strouse, C. E.; Hanson, L. K.; Valentine, J. S. [Peroxotetraphenylporphinato]manganese(iii) and [Chlorotetraphenylporphinato]manganese(ii) Anions - Syntheses, Crystal-Structures, and Electronic-Structures. *J. Am. Chem. Soc.* **1987**, *109*, 1425-1434.
(40) Horcas, I.; Fernandez, R.; Gomez-Rodriguez, J. M.; Colchero, J.; Gomez-Herrero, J.; Baro, A. M. WSXM: A software for scanning probe microscopy and a tool for nanotechnology. *Rev. Sci. Instrum.* **2007**, *78*, 013705.

(41) Hermann, K.; Van Hove, M. A. LEED pattern simulator LEEDpat Version 2.1 (2006). http://www.fhi-berlin.mpg.de/KHsoftware/LEEDpat/index.html.
(42) Adler, A. D.; Longo, F. R.; Kampas, F.; Kim, J. On preparation of metalloporphyrins. *J. Inorg. Nucl. Chem.* **1970**, *32*, 2443-2445.